THE ASTROPHYSICAL JOURNAL, 454:370–381, 1995 November 20

ACCRETING, ISOLATED NEUTRON STARS. III. PREHEATING OF INFALLING GAS AND COMETARY H II REGIONS

OMER BLAES[1] AND ORLANDO WARREN[2]
Department of Physics, University of California, Santa Barbara, CA 93106
AND
PIERO MADAU[3]
Space Telescope Science Institute, 3700 San Martin Drive, Baltimore, MD 21218
Received 1995 March 23; accepted 1995 May 31

ABSTRACT

Nearby, isolated, old neutron stars (IONSs) accreting interstellar material might be detectable as sources of UV and soft X-ray radiation. We investigate the interaction between this radiation field and the surrounding medium, assumed to consist of purely hydrogen and helium. This interaction results in a cometary H II region around the star which we model in detail by including all the relevant time-dependent ionization, recombination, heating, and cooling processes. We find that preheating of the ambient gas to temperatures higher than 10^4 K may significantly quench the accretion rate onto these neutron stars, thereby reducing the IONS number counts in the EUV and soft X-ray bands predicted by previous investigations. However, the reprocessing of hard radiation by the surrounding H II regions may enhance the detectability of IONSs at optical wavelengths. Searches for nearby accreting IONSs are currently being undertaken.

Subject headings: accretion: accretion disks — H II regions — stars: neutron — ultraviolet: stars — X-rays: stars

1. INTRODUCTION

Neutron stars are typically observed through nonthermal emission as pulsars, through X-ray emission from rapid accretion in binary systems, and possibly through gamma-ray emission in the three known soft gamma-ray repeaters. However, the vast majority of neutron stars in the Galaxy remain undetected, since those which started out as ordinary, isolated radio pulsars are now in general far too old to emit detectable pulsed radio emission. The Galaxy is believed to contain $N_{\rm tot} \simeq 10^8$–10^9 such dead pulsars. Given the expected local space density, about 10^{-4} $(N_{\rm tot}/10^8)$ pc^{-3} (Paczyński 1990; Blaes & Madau 1993), the nearest such star is only ~ 10 pc away. For comparison, the nearest observed pulsars are ~ 100 pc away (Taylor, Manchester, & Lyne 1993). As first discussed by Ostriker, Rees, & Silk (1970), these nearby, isolated, old ($\sim 10^{10}$ yr) neutron stars might be detectable by the radiation released from the accretion of interstellar material. This possibility has received renewed interest because the *ROSAT* and *Extreme-Ultraviolet Explorer* (*EUVE*) all-sky surveys have recently achieved the required sensitivity (Treves & Colpi 1991; Blaes & Madau 1993; Colpi, Campana, & Treves 1993; Madau & Blaes 1994). A successful detection of these IONSs would provide a unique probe of the star formation and chemical enrichment history of the Galaxy and the long-term evolution of neutron stars. Interesting candidate sources are already known, e.g., the X-ray source MS 0317.7−6647 (Stocke et al. 1995).

This is the third paper in a series aimed at assessing the observability of accreting IONSs as sources of optical/UV and X-ray radiation. In Paper I (Blaes & Madau 1993), we presented a detailed calculation of the kinematic properties of the IONS population in the solar neighborhood and estimated the numbers of sources which would be detectable in the *ROSAT*/*EUVE* all-sky surveys. Assuming blackbody emission and $N_{\rm tot} = 10^8 N_8$ neutron stars in the Galaxy, we estimated that, in the case of isotropic accretion over the entire stellar surface, about $200N_8$ accreting IONSs should have been detected in the *ROSAT* PSPC all-sky survey, with $\sim 60N_8$ of them showing up in the *ROSAT* Wide-Field Camera (WFC) and *EUVE* surveys. An accretion flow channeled onto 1 km^2 magnetic polar caps produces instead $\sim 1000N_8$ detectable X-ray sources in the PSPC survey, and only $\sim 10N_8$ EUV sources in the WFC and *EUVE* surveys.

In Paper II (Madau & Blaes 1994) we improved on the analysis of Paper I by including the effects of dynamical heating of the IONS population.[4] The scattering of IONSs by molecular clouds, spiral arms, and whatever else might be responsible for the increase in velocity dispersion with age observed in the local disk population of stars (e.g., Wielen 1977) heats, over the lifetime of the Galaxy, the low-velocity IONSs to higher speeds, thereby reducing by up to a factor of 10 the predicted source number counts (as low-velocity IONSs have the highest accretion luminosities).

In this paper we examine the interaction between the ionizing radiation field of the star and the surrounding medium. As we first suggested in Paper I, a portion of this radiation will be reprocessed to form a cometary H II region. A study of such regions is important for three reasons. First, detectability requires the flow to be hydrodynamic so that accretion occurs in the Bondi-Hoyle regime. This will only occur if the medium is ionized out to the accretion radius, which can only be accomplished in neutral media by photoionization by the

[1] blaes@vela.physics.ucsb.edu.
[2] orlando@sbphy.physics.ucsb.edu.
[3] madau@stsci.edu.

[4] We also adopted a more definite global model of the interstellar medium consisting of a low-density spherical cavity embedded in a higher density homogeneous slab. This alone altered the predictions of Paper I by factors of 1.3–4.

stellar radiation field itself. Second, the accretion rate is sensitive to the sound speed at the accretion radius, which in our previous calculations was simply assumed to be 10 km s^{-1}. This is typical of UV-photoionized gas at $\sim 10^4$ K, such as in static H II regions around early-type stars. However, the radiation field of an IONS is much harder and could preheat the ambient gas to higher temperatures, *thereby quenching the accretion rate*. In addition, the motion of the star relative to the ambient medium can cause the cooling time of the accreting material to exceed both the flow and the heating times. Hence, the sound speed must be determined self-consistently. It is exactly this time-dependent preheating of the accretion flow which we wish to examine here in detail. Finally, given the possibility that IONSs may be lurking among the unidentified sources in the surveys, it is important to devise an observational strategy to detect them. At first, this may appear to be an impossible task. Assuming that the surface emission is thermal, IONSs are expected to be extremely faint in the optical ($B > 25.6$ at a distance of 100 pc, the characteristic size of the local bubble; see Paper II). Because the error boxes associated with sources detected in the mentioned sky surveys are so large (of order a few arcminutes), confusion is a serious obstacle to searches at such deep limiting magnitudes. We shall see, however, that reprocessing by the H II region may enhance the detectability of IONSs at wavelengths longer than the EUV, thereby aiding identification.

Detailed modeling of cometary H II regions including all the time-dependent ionization, recombination, heating, and cooling processes associated with the constituent elements of the gas is an ambitious undertaking. In this paper we shall consider the model problem of a medium free of dust and metals. Beyond its pedagogical importance, a detailed numerical modeling of cometary H II regions in a medium consisting of pure hydrogen and helium may provide reasonably complete answers to the questions of preionization and preheating, as well as a partial description of the reprocessed spectrum. The plan of the paper is as follows. In § 2 we present simple analytic estimates of the hydrogen ionization structure of the nebulae in both the optically thin and thick limits. In § 3 we discuss the equations and assumptions of our numerical models. The actual model results are presented in § 4, where we also show how the preheating of the ambient gas by emergent soft X-rays can quench accretion onto a neutron star, thereby significantly reducing the predicted IONS number counts. We estimate continuum and emission-line luminosities from such nebulae in § 5 and summarize our conclusions in § 6. Although our emphasis is on the ionization nebulae surrounding IONSs accreting from the interstellar medium (ISM), the formalism we develop and our results can also be applied to the interaction of any discrete source of EUV/soft X-ray radiation with the ambient medium, such as, e.g., the H II regions produced by the luminous supersoft X-ray sources recently detected by *ROSAT* (Rappaport et al. 1994), or low-luminosity, wind-fed X-ray binaries. We note that a crude analysis which first touched on many issues that we discuss here was done some time ago by Shvartsman (1971).

2. SIMPLE ESTIMATES OF IONIZATION STRUCTURE

If the flow is adiabatic, the accretion rate is given by

$$\dot{M} = \frac{4\pi\lambda_a G^2 M_*^2 \rho}{(v^2 + c_s^2)^{3/2}} \tag{1}$$

(Bondi 1952; Hunt 1971; Ruffert & Arnett 1994), where M_* is the star mass, $v_i \equiv 20 v_{20}$ km s^{-1} is the speed of the neutron star relative to the interstellar medium, and c_s and $\rho = n m_p$ are the sound speed and the interstellar mass density at infinity, respectively. We take the neutron star to have mass $M_* = 1.4\ M_\odot$ and radius $R_* = 10$ km. The accretion eigenvalue λ_a is unity for supersonic accretion. The accretion luminosity of the star is

$$L = \frac{G M_* \dot{M}}{R_*} \simeq 1.7 \times 10^{31} n V_{20}^{-3} \text{ ergs s}^{-1}\ , \tag{2}$$

where $V \equiv (v^2 + c_s^2)^{1/2} \equiv 20 V_{20}$ km s^{-1}. In the following, we shall assume that the stellar emission spectrum is a blackbody with temperature T_* and emitting area $A \equiv 10^3 A_3$ km^2. For polar cap accretion, we assume that the magnetic axis is misaligned with the rotation axis and the star is rotating sufficiently rapidly that the stellar emission is isotropic on all timescales of interest. (In practice, this requires the rotation period to be much less than a year; see eq. [4] below.)

Provided $V \ll 70 n^{1/3} A_3^{-1/3}$ km s^{-1}, which will be true of all detectable IONSs in the sky surveys (Paper II), then the hydrogen Lyman edge is in the Rayleigh-Jeans region of the stellar spectrum, and the rate of emission of ionizing photons by the star is given by

$$S \simeq 1.1 \times 10^{41} n^{3/4} V_{20}^{-9/4} A_3^{1/4} \text{ s}^{-1}\ . \tag{3}$$

We shall assume that the gas is neutral and homogeneous far ahead of the star. Gravitational focusing of the gas will be negligible on scales larger than the accretion radius, which we crudely define as

$$R_{\rm acc} \equiv \frac{G M_*}{V^2} \simeq 5 \times 10^{13} V_{20}^{-2} \text{ cm}\ . \tag{4}$$

This radius is very small compared to the scales of the nebula discussed below. Throughout this paper, we shall therefore simply take the gas to stream by the star on straight line trajectories. Provided $V \lesssim 300 n^{1/10} B_{12}^{-1/5}$ km s^{-1}, where $B = 10^{12} B_{12}$ G is the surface magnetic field of the star, the Alfvén radius will be inside the accretion radius and the influence of the star's magnetic field on the flow will also be negligible.

For the purposes of making simple estimates of the nebular ionization structure, we assume for the remainder of this section that the gas consists of pure hydrogen. We can define three important characteristic length scales in the nebula. The photon mean free path at the Lyman edge in neutral gas is

$$R_{\rm abs} \equiv \frac{1}{n\sigma_0} = 1.6 \times 10^{17} n^{-1} \text{ cm}\ , \tag{5}$$

where $\sigma_0 = 6.3 \times 10^{-18}$ cm^2 is the photoionization cross section of the ground state of hydrogen at threshold. We can also define an ionization length scale

$$R_i \equiv \frac{1}{4\pi v} \int_{\nu_0}^{\infty} d\nu \sigma_{\rm H}(\nu) \frac{A \pi I_\nu(R)}{h\nu} < \frac{S\sigma_0}{4\pi v} = 2.8 \times 10^{16} n^{3/4} V_{20}^{-9/4} v_{20}^{-1} A_3^{1/4} \text{ cm} \tag{6}$$

(Alcock & Illarionov 1980; Verdon et al. 1991), where $I_\nu(R) = B_\nu(T_*)$ is the specific intensity at the surface of the star and $\sigma_{\rm H}(\nu)$ is the hydrogen photoionization cross section. The velocity dependence of R_i reflects the fact that at high velocities there is

a smaller probability of a given fluid element being ionized as it flows past the star. Finally,

$$R_r \equiv \frac{v}{\alpha_B n} = 7.7 \times 10^{18} n^{-1} v_{20} \text{ cm} \quad (7)$$

is a recombination length scale (Alcock & Illarionov 198[illegible]). Here $\alpha_B = 2.6 \times 10^{-13}$ cm^3 s^{-1} at 10^4 K is the hydrogen recombination coefficient to the excited bound states. At high velocities, ionized gas will extend farther out into a long tail downwind of the star before recombining.

2.1. *Optically Thick Limit*

If most of the ionizing radiation is emitted near threshold and $R_{\rm abs} \ll R_i$, the photon mean free path is short in the neutral gas and the ionization front near the star may be taken to be perfectly sharp, i.e., the Strömgren approximation is valid ("ionization-bounded nebula"). The usual Strömgren radius is

$$R_s \equiv \left(\frac{3S}{4\pi n^2 \alpha_B}\right)^{1/3} \simeq 4.6 \times 10^{17} n^{-5/12} V_{20}^{-3/4} A_3^{1/12} \text{ cm} \quad (8)$$

and is the characteristic size of the nebula produced by a slowly moving star. Note that $R_s \sim (R_i R_r R_{\rm abs})^{1/3}$.

Many neutron stars will be moving fast enough to cross their Strömgren radius in much less than a recombination time, i.e., $R_r \gg R_s$ or $n \ll 120 V_{20}^{9/7} v_{20}^{12/7} A_3^{-1/7}$ cm^{-3}. In this regime, the ionized region is stretched into a long, thin cometary shape (Raga 1986; Paper I). The shape of the ionization front near the star is given by (Rasiwala 1969; Paper I)

$$R(\theta) = \left[\frac{2R_s^3}{3R_r(1+\cos\theta)}\right]^{1/2}, \quad (9)$$

where θ is the polar angle measured from the direction of motion of the star. The distance of the ionization front directly ahead of the star is therefore

$$R(0) = \left(\frac{R_s^3}{3R_r}\right)^{1/2} \simeq 6.6 \times 10^{16} n^{-1/8} V_{20}^{-9/8} v_{20}^{-1/2} A_3^{1/8} \text{ cm} . \quad (10)$$

Note that $R(0) \sim (R_i R_{\rm abs})^{1/2}$ and is independent of the recombination coefficient. The diffuse radiation field is therefore not important in determining the ionization structure near the star. The maximum transverse size of the ionized region is $4R(0)$. Behind the star, the gas slowly recombines in a long tail of distance $\sim R_r$.

With the chosen scalings, equations (5) and (10) imply that $R_{\rm abs} > R(0)$. This will in general be true for ambient densities $n \lesssim 3 V_{20}^{9/7} v_{20}^{4/7} A_3^{-1/7}$ cm^{-3}. If most of the ionizing photons are emitted well above threshold, the ionization front will not be sharp and the Strömgren approximation will be invalid even in high-density environments.

2.2. *Optically Thin Limit*

In a low-density medium, $R_{\rm abs} \gg R_i$ and photon absorption may be neglected when calculating the ionization structure near the star ("matter-bounded nebula"). Provided $R_r \gg R_i$, or $n \ll 25 V_{20}^{9/7} v_{20}^{8/7} A_3^{-1/7}$ cm^{-3}, the nebula will again have a cometary shape with length $\sim R_r$, but now the transverse width $\sim R_i$. Because photon mean free paths are larger than the transverse width, we neglect the diffuse radiation field produced by the recombinations in the tail when considering the structure near the symmetry axis.

Consider a fluid element on a trajectory making impact parameter b away from the neutron star. The change in number density $n_{\rm H\,II}$ of ionized atoms along the trajectory is given by

$$\left(\frac{\partial f}{\partial x}\right)_b = \frac{1-f}{b^2+x^2} R_i - \frac{f^2}{R_r'}, \quad (11)$$

where $f \equiv n_{\rm H\,II}/n$ is the ionization fraction ($0 \le f \le 1$), x is the distance of the gas element behind the star projected onto the symmetry axis, and $R_r' \equiv v/(\alpha_A n)$ is the recombination length scale redefined to include recombinations to the ground state ($R_r' \simeq 0.6 R_r$ at 10^4 K).

If $R_r' \gg R_i$, it is a good approximation to neglect the effects of recombinations ahead of the star and on scales $\ll R_r'$ downwind of the star. In this region, equation (11) implies

$$f = \begin{cases} 1 - \exp\left[R_i/b \, \tan^{-1}(b/x)\right] & x \le 0 , \\ 1 - \exp\left\{R_i/b \, [\tan^{-1}(b/x) - \pi]\right\} & x \ge 0 . \end{cases} \quad (12)$$

Note that for $R_i \ll x \ll R_r'$, equation (12) implies $f \simeq 1 - \exp(-\pi R_i/b)$ and, as expected, significant ionization occurs only for $b \lesssim R_i$. (Eq. [12] provides a poor approximation to the neutral fraction $1-f$ *very* near the star, because recombinations can balance ionizations when the neutral fraction is very low.) Behind the star, for $x \gg R_i$, we may neglect ionizations, and equation (11) gives $f = 1/[C(b) + x/R_r']$. The function $C(b)$ may be determined by matching to the solution of equation (12), giving

$$f = \frac{1 - \exp(-\pi R_i/b)}{1 + (x/R_r')[1 - \exp(-\pi R_i/b)]} . \quad (13)$$

As expected, $f \to 0$ as $x/R_r' \to \infty$, so the cometary H II region will extend a distance $\sim R_r'$ downwind of the neutron star. Equation (11) also describes the nebular structure near the star if it is moving at very low velocities, provided again that photon mean free paths are large. In this regime, the left-hand side may be neglected, implying

$$f = \frac{(R_i^2 R_r'^2 + 4R_i R_r' R^2)^{1/2} - R_i R_r'}{2R^2} , \quad (14)$$

where $R = (b^2 + x^2)^{1/2}$ is the distance from the star. At large radii, $f \to (R_i R_r')^{1/2}/R$, and the characteristic radius of the ionized region becomes $(R_i R_r')^{1/2}$. The estimates made in this section will be used to understand the more detailed numerical modeling of the nebulae, to which we now turn.

3. EQUATIONS AND ASSUMPTIONS

3.1. *Ionization and Thermal Structure of the Nebula*

We shall assume that the ambient gas consists of atomic hydrogen and helium, with helium being 9.8% abundant relative to hydrogen by number (Grevesse & Anders 1989). We neglect the effects of both dust and metals.

As before, the gas is assumed to be neutral and homogeneous far ahead of the star and to flow by on straight trajectories at constant speed. The differential equations describing

the ionization and thermal structure of the nebula are given by

$$v\left(\frac{\partial n_{\rm H\,II}}{\partial x}\right)_b = \mathscr{I}({\rm H\ I}) - \mathscr{R}({\rm H\ II})\,, \quad (15)$$

$$v\left(\frac{\partial n_{\rm He\,II}}{\partial x}\right)_b = \mathscr{I}({\rm He\ I}) - \mathscr{R}({\rm He\ II}) - \mathscr{I}({\rm He\ II}) + \mathscr{R}({\rm He\ III})\,, \quad (16)$$

$$v\left(\frac{\partial n_{\rm He\,III}}{\partial x}\right)_b = \mathscr{I}({\rm He\ II}) - \mathscr{R}({\rm He\ III})\,, \quad (17)$$

and

$$v\left(\frac{\partial T}{\partial x}\right)_b = \frac{2(\mathscr{H} - \mathscr{C})}{3k(n_{\rm H} + n_{\rm He} + n_e)}\,. \quad (18)$$

Here $\mathscr{I}$ and $\mathscr{R}$ are the ionization and recombination rates, respectively, associated with each ionization state, $\mathscr{H}$ is the heating rate, and $\mathscr{C}$ is the cooling rate. Collisions are assumed to be rapid enough to ensure that all components of the plasma are at the same temperature T. The number density of each ionization state is denoted by n with an appropriate subscript, while $n_{\rm H}$, $n_{\rm He}$, and n_e denote the total hydrogen, helium, and electron number densities, respectively. The last is determined by $n_e = n_{\rm H\,II} + n_{\rm He\,II} + 2n_{\rm He\,III}$. The total baryon density used to calculate the accretion rate in equation (1) is $n = n_{\rm H} + 4n_{\rm He}$.

Nearly all the formulae which we use for the ionization, recombination, heating, and cooling rates for a pure hydrogen and helium gas are conveniently summarized by Cen (1992). Photoionization, collisional ionization by free electrons, recombination, and dielectronic recombination of He II are all included in $\mathscr{I}$ and $\mathscr{R}$. Heating is due solely to photoionization and Compton upscattering, while the processes contributing to cooling are collisional ionization, recombination, dielectronic recombination of He II, collisional excitation, bremsstrahlung, and Compton downscattering. The photoionization cross section of He I given by Osterbrock (1989) is a poor approximation at high photon energies, and we use instead the following fitting formula based on the numerical data of Reilman & Manson (1979) (see Haardt & Madau 1995):

$$\sigma_{\rm He\,I} = \frac{0.6935 \times 10^{-18}}{E^{1.82} + E^{3.23}}\ {\rm cm}^2\,, \quad (19)$$

for $E > 0.26$, where E is the photon energy in units of 100 eV.

For high accretion rates and small emitting areas, neutron stars can emit significant numbers of X-ray photons. We have therefore included the effects of secondary ionizations by energetic photoelectrons according to the prescriptions given by Shull & Van Steenberg (1985). Specifically, in order to reduce the contribution to photoionization heating by photoelectrons with energies >100 eV we multiply the uncorrected rates by a factor

$$0.9971\left\{1 - \left[1 - \left(\frac{n_{\rm H\,II}}{n_{\rm H}}\right)^{0.2663}\right]^{1.3163}\right\}. \quad (20)$$

The additional ionization rate of H I is given by multiplying the uncorrected photoionization heating rate by

$$\frac{0.3908}{h\nu_{\rm H}}\left[1 - \left(\frac{n_{\rm H\,II}}{n_{\rm H}}\right)^{0.4092}\right]^{1.7592}. \quad (21)$$

The corresponding multiplication factor for He I is

$$\frac{0.0554}{h\nu_{\rm He\,I}}\left[1 - \left(\frac{n_{\rm H\,II}}{n_{\rm H}}\right)^{0.4614}\right]^{1.6666}, \quad (22)$$

where $h\nu_{\rm He\,I}$ is the ionization energy of He I. Secondary ionizations of He II are not important. These formulae provide adequate approximations for photoelectron energies greater than 100 eV. Strictly speaking, even electrons with energy less than 100 eV can contribute to secondary ionization, but they are individually less efficient at doing so than higher energy electrons (Shull & Van Steenberg 1985).

Different regions of the nebula will generally be coupled together through the diffuse ionizing radiation field and optical depth effects. These may be included in an iterative manner by storing the temperature and ionization structure on a discrete grid in x and b. For simplicity we adopt a uniform grid, and because comparable resolution may be required near the ionization fronts in both directions, we choose the grid spacings in x and b to be the same. Trajectories are integrated along grid lines of constant b using an accurate, variable step size Runge-Kutta algorithm to go from one x grid point to the next. This enables us to calculate accurately the nebular structure near the star where the density and temperature may be changing on a scale much smaller than the grid resolution, but where absorption and the diffuse radiation field are negligible. We do not calculate a trajectory along the symmetry axis, but rather one displaced slightly away by an impact parameter equal to the accretion radius or a tenth of the grid spacing, whichever is smaller. We start our iterations off by taking the gas to be neutral everywhere and to have a temperature of 100 K. (We also always take these to be the initial conditions ahead of the star.) After calculating absorption columns between every grid point and the star, we proceed to integrate the gas trajectories, recalculate the absorption columns, and iterate to convergence. In practice, this typically requires only a few iterations. We have also found that calculation of the diffuse radiation field, along with its radiative transfer, is enormously expensive computationally. Therefore, we have neglected it entirely when computing the nebular structure. Instead we have limited ourselves to calculating the diffuse radiation in various regions of the converged nebula, checking to make sure that its contribution to the heating and ionization rates is negligible. This is generally true ahead of the star but *not* always true behind the star. We shall discuss this in more detail in § 4, which deals with some specific cases.

3.2. *Accretion Rate*

Equation (1) for the accretion rate is valid only for flows which are adiabatic (away from shocks) with specific heat ratio $\gamma = 5/3$ and with a perfectly absorbing boundary condition at the stellar surface. The accretion flow is actually quite sensitive to the inner boundary condition, even in the adiabatic case (e.g., Fryxell, Taam, & McMillan 1987). As a result of the immense gravitational potential and the collisionless nature of the flow at these low accretion rates near the surface of the neutron star, a perfectly absorbing boundary condition is probably accurate, provided the magnetic field of the star is weak. If the star is magnetized and spinning rapidly, then the propeller mechanism may be efficient in blocking the accretion flow. However, we have argued in Paper I that this is unlikely for IONSs because they should spin down sufficiently to allow accretion to occur.

More problematic is the assumption of an adiabatic flow, which is clearly violated in our case as a result of the nonequilibrium heating and cooling which occurs on scales much larger than the accretion radius. Other specific heat ratios apart from $\gamma = 5/3$ have been explored by Hunt (1979) and

Shima et al. (1985). However, these calculations neglect radiative heating and cooling and still assume that γ is constant. Much work has been done on spherical accretion with non-equilibrium heating and cooling (e.g., Ostriker et al. 1976; Cowie, Ostriker, & Stark 1978; Krolik & London 1983; Nobili, Turolla, & Zampieri 1991), and this has shown that preheating and radiation pressure may both inhibit the accretion flow and produce time-dependent behavior. However, none of these studies address the low-luminosity regime of interstellar accretion onto IONSs, nor do they self-consistently include all the complex atomic processes which are relevant to this case. Taam, Fu, & Fryxell (1991) have conducted full numerical simulations of accretion from axisymmetric flows including Compton heating/cooling and bremsstrahlung cooling. At accretion rates much less than the Eddington rate, the flow is approximately adiabatic, but the neglect of atomic processes precludes application of these results to the present problem.

A full hydrodynamic simulation of the accretion flow is beyond the scope of this paper, and we limit ourselves to examining whether preheating *might* be important in inhibiting accretion. We therefore adopt equation (1) for the accretion rate. We must still specify the sound speed, which in adiabatic steady flow is evaluated at infinity but in our case with preheating is probably best taken to be the value at a point where gravity starts to affect the flow, i.e., at the accretion radius. Hence, we take

$$c_s = \left[\frac{5kT(n_{\rm H} + n_{\rm He} + n_e)}{3nm_p}\right]^{1/2}, \tag{23}$$

where m_p is the mass of the proton. As we iterate the nebular structure, the sound speed will change. The values of the temperature and density which we insert in equation (23) are taken at $x = 0$ and an impact parameter equal to the *old* accretion radius (interpolation is required if the grid is so fine that the trajectory closest to the symmetry axis passes inside the accretion radius). We use the new sound speed in equation (1) to iterate on the accretion rate as well, so that the converged nebula represents a self-consistent solution for the accreting neutron star. It turns out that c_s can become comparable to the neutron star velocity v, in which case the accretion eigenvalue λ_a is no longer unity. We have fitted the numerical data of Hunt (1971) to about 10% by the following formula:

$$\lambda_a = \frac{(v^2 + c_s^2)^{3/2}}{(v^6 + 16c_s^6)^{1/2}}. \tag{24}$$

This reproduces the expected behavior that $\lambda_a = \frac{1}{4}$ at $v = 0$ and $\lambda_a = 1$ as $v \to \infty$. We have used this equation to calculate λ_a in equation (1) when iterating on the accretion rate.[5]

Note that one should not take our results for the accretion rate below too seriously, since our prescription is only phenomenological. In particular, if the sound speed shows steep variation near the accretion radius (both with distance and around the star), then our approach would be in serious trouble. We discuss this further below in § 4.4. A full non-adiabatic, hydrodynamic simulation of the accretion flow is necessary to resolve these issues rigorously.

[5] The referee has informed us that another interpolation formula has been proposed and tested recently by Ruffert (1994) and Ruffert & Arnett (1994). Their interpolation formula agrees with ours to within 40%.

4. NEBULAR STRUCTURE

4.1. *An Optically Thick Nebula*

Figure 1 depicts the temperature and ionization structure of the nebula created by an isotropically accreting neutron star moving at $v = 20$ km s^{-1} through an $n = 100$ cm^{-3} medium, typical of dense molecular clouds. The grid used for calculating absorption and determining convergence had 401 points equally spaced between $x = \pm 5 \times 10^{17}$ cm and 201 points equally spaced from near the symmetry axis to 5×10^{17} cm. The sound speed at the accretion radius converged to 23 km s^{-1}, giving an accretion rate of 1×10^{12} g s^{-1}. Figure 2 depicts the run of sound speed with distance along several cuts parallel to the symmetry axis of the nebula. The maximum sound speed actually occurs somewhat behind the star, and the flow is barely subsonic near the star. However, throughout most of the nebula the flow is supersonic. Given that the sound speed in the tail is $\simeq 10$ km s^{-1} near the symmetry axis, and that it decreases transversely over a scale $\sim 10^{17}$ cm, we would expect transverse expansion to occur in the tail after a distance $\sim 2 \times 10^{17}$ cm behind the star. Because we neglect hydrodynamic effects, our numerical modeling becomes dubious beyond this point.

The ionization length scale is $R_i \simeq 3 \times 10^{15}$ cm, which is somewhat greater than the absorption length at threshold, $R_{\rm abs} \simeq 2 \times 10^{15}$ cm. Hence, this case is marginally optically thick in the sense described in § 2.1, and Figure 1 shows that equation (9) provides a fair approximation to the hydrogen ionization front near the star. The hydrogen recombination length is $\sim 10^{17}$ cm, and so the H II density starts to decay over this length scale in the tail. The region of singly ionized helium is significantly more extended than the hydrogen ionization zone, a feature which is generic to all our $v = 20$ km s^{-1} simulations. This is a result of the hard spectrum of the neutron star as compared to ordinary hot stars; the surface temperature in this case is $\simeq 8 \times 10^5$ K. Similar morphology is evident in the static, spherical model nebulae for supersoft X-ray sources calculated by Rappaport et al. (1994).

In contrast to hydrogen, the He II and He III contours have a winged morphology. This is because of the three ionization states of helium. Along the symmetry axis, all the helium is fully ionized as it passes the star, beyond which it starts to recombine to He II and He I. Away from the symmetry axis, the ionizing radiation flux does not achieve the same intensity, and it takes somewhat longer to ionize to He II and subsequently to He III. The maximum abundance of He III is therefore reached behind the star, after which it recombines to produce a source of He II well behind the star, creating the extended wings in the He II contours.

The diffuse ionizing radiation field, which we have neglected in our simulations, significantly modifies the structure of static, optically thick H II regions. To check what possible effects this might have here, we have calculated a posteriori the heating and H I ionization rates at various positions within the converged nebula as a result of the diffuse Lyman continuum radiation produced from hydrogen recombination, including optical depth effects. We find that along the symmetry axis ahead of the star, the H I ionization rate produced by the diffuse field is less than 0.5% of that caused by the primary photons emitted by the star, and the diffuse heating rate was even more negligible. Our neglect of diffuse radiation is therefore a good approximation ahead of the star, because the gas flows by before it has a chance to recombine. We expect this to

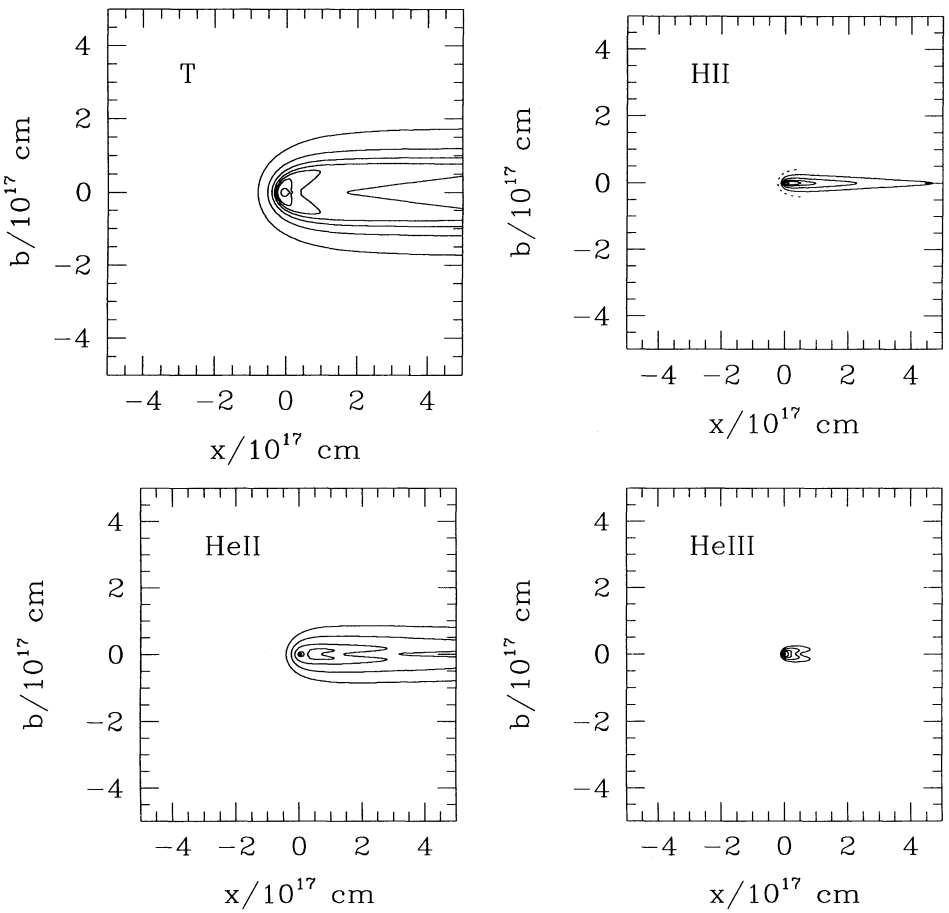

FIG. 1.—Nebular structure for isotropic accretion onto a neutron star moving at $v = 20$ km s^{-1} through a medium with $n = 100$ cm^{-3}. Temperature contours are from 2000 K to 14,000 K in steps of 2000 K. Ionization fraction contours are 0.1, 0.2, 0.4, 0.6, and 0.9. The dashed curve in the H II plot is the Strömgren surface according to equation (9).

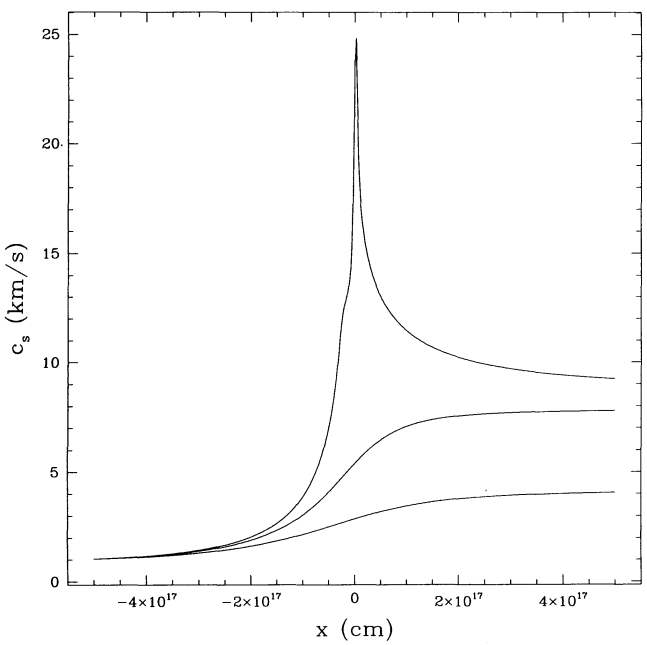

FIG. 2.—Sound speed as a function of distance parallel to the symmetry axis for the same case as shown in Fig. 1. From top to bottom, the curves are for impact parameters of 2×10^{13} cm (the accretion radius), 10^{17} cm, and 2×10^{17} cm.

be an even better approximation for larger velocities or lower densities, both of which increase the recombination length scale R_r. Behind the star, however, the diffuse radiation field becomes increasingly important, and it quickly dominates the ionization rate. (However, it never dominates the heating rate because of the lower energy photons.) Diffuse recombination photons may therefore contribute to increasing the size of the ionized tail.

Along the symmetry axis, photoionization heating is orders of magnitude larger well ahead of the star than all the cooling processes combined. This starts to change at a distance of $\simeq 4 \times 10^{16}$ cm, when the temperature gets high enough that collisional excitation and ionization cooling of hydrogen kicks in. At a distance of $\simeq 2 \times 10^{16}$ cm ahead of the star, the gas reaches complete thermal equilibrium. This then breaks down as soon as the star is passed and the cooling exceeds the heating. Ionization equilibrium, however, is never achieved. The ionization rate of hydrogen exceeds the recombination rate by at least an order of magnitude ahead of the star, while behind the star the recombination rate dominates. *The lack of ionization and thermal equilibrium is a generic feature of all the nebulae that we have simulated.*

4.2. *An Optically Thin Nebula*

Figure 3 depicts the nebula formed around an isotropically accreting star again moving at $v = 20$ km s^{-1}, but now through an $n = 1$ cm^{-3} medium. The grid used here had 401

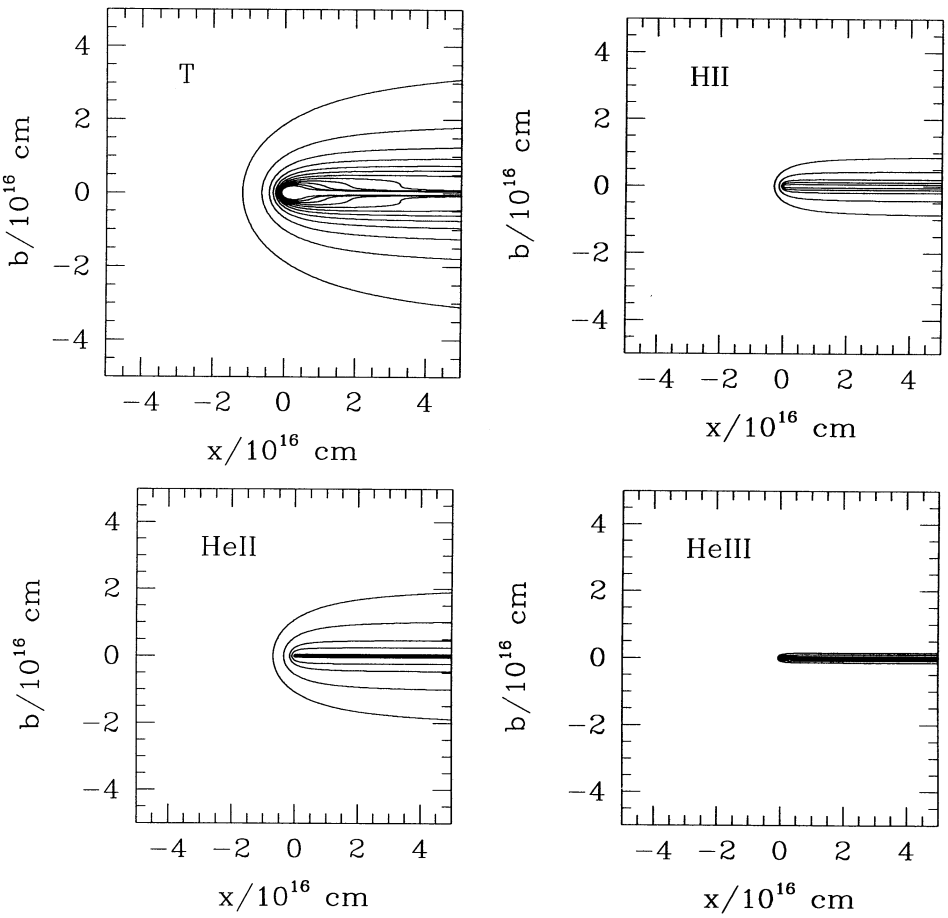

FIG. 3*a*

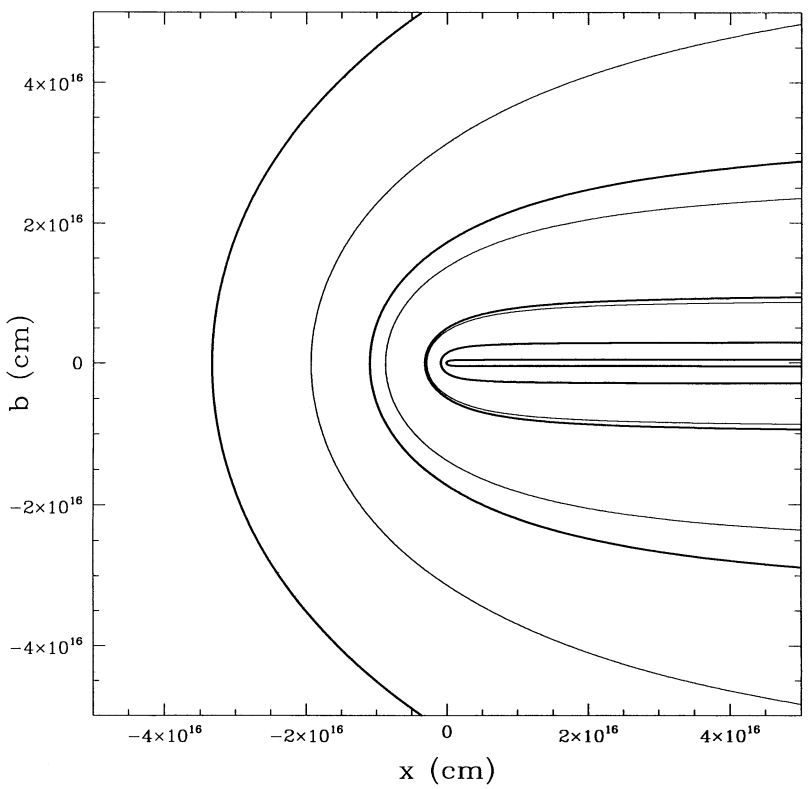

FIG. 3*b*

FIG. 3.—(*a*) Nebular structure for isotropic accretion onto a neutron star moving at $v = 20$ km s^{-1} through a medium with $n = 1$ cm^{-3}. Temperature contours are from 2000 K to 24,000 K in steps of 2000 K. Ionization fraction contours are the same as in Fig. 1. (*b*) Contours of $n_{\rm H\,II}/n_{\rm H}$ at values of 0.01, 0.03, 0.1, 0.3, and 0.9. Light curves are results from the numerical calculations, while heavy curves are the optically thin analytic approximation given by eq. (12).

points equally spaced between $x = \pm 5 \times 10^{16}$ cm and 201 points equally spaced from near the symmetry axis and $b = 5 \times 10^{16}$ cm. We also simulated this case on a 401 by 201 grid which was 10 times larger. In both cases the sound speed at the accretion radius converged to 35 km s^{-1}, giving an accretion rate of 4×10^9 g s^{-1}. The sound speed near the symmetry axis is well above the flow speed in the portion of the tail on our grid. Note that the tail in this case is expected to extend far beyond the grid, as the recombination length scale $R_r' \sim 5 \times 10^{18}$ cm. We have not attempted to simulate this region, which in any case will be subject to thermal expansion. The sound speed decreases transversely on a scale of several times 10^{15} cm, so that transverse hydrodynamic expansion will occur on a slightly smaller scale behind the star.

The temperature distribution shows that cooling in the tail is much more effective just off the symmetry axis than on it. The reason for this is that the hydrogen is fully ionized on the axis, and hydrogen collisional excitation and ionization cooling is not possible. Both because the gas away from the symmetry axis is not as completely ionized and because the recombination coefficient is higher at the lower temperatures, these cooling processes do operate here. The same effect is evident in the innermost temperature contours shown in Figure 1.

This nebula is optically thin, and its hydrogen ionization structure should therefore be well approximated by the simple analytic theory of § 2.2. Figure 3*b* shows a detailed comparison between the numerically calculated H II fraction contours and those predicted by equation (12). The agreement is nearly perfect for the highest ionization inner contours. The agreement between the outer contours is significantly improved for the simulation done on the larger grid. The difference between the numerical and analytic results at low ionization fractions is therefore largely due to the artificial initial data of a completely neutral medium at the edge of the grid.

4.3. *A Case with Hard Photons*

Figure 4 depicts the nebular structure for a neutron star which is again moving at $v = 20$ km s^{-1} through an $n = 100$ cm^{-3} medium, but which is accreting onto a magnetically confined surface area of 1 km^2. The calculations were again done on a uniform, 401 × 201 grid, covering the region $\pm 5 \times 10^{15}$ cm around the neutron star. Lower resolution, larger grids were also tried with very little change in the results. The sound speed at the accretion radius in these simulations converged to 36–39 km s^{-1}, giving an accretion rate of $3 - 4 \times 10^{11}$ g s^{-1}. The hydrogen recombination length scale is still $\sim 10^{17}$ cm, which is far downstream of the grid used to generate Figure 4. The larger grid simulations do, however, confirm that recombination occurs on this scale. The temperature distribution again shows the persistent hot region of gas along the symmetry axis in the tail, as a result of the absence of hydrogen collisional excitation and ionization cooling in this region.

The ionization length scale in this case is only $R_i \simeq 1 \times 10^{13}$ cm. This is much less than the value at threshold, $\sim S\sigma_0/(4\pi v)$, and is due to the predominantly hard photons being emitted by the hot ($\simeq 3 \times 10^6$ K) stellar surface. The nebula is therefore optically thin, and Figure 4*b* shows a comparison between the numerical hydrogen ionization structure and equation (12). The agreement is good, but the simulation produces somewhat more extended ionization. This is almost entirely due to the secondary ionizations produced by energetic photoelectrons. A simulation in which these were neglected showed much better agreement with the analytic theory of § 2.2.

4.4. *Impact of Preheating on IONS Number Counts*

In all the cases discussed above, the sound speed at the accretion radius is substantially larger than the 10 km s^{-1} assumed in Papers I and II. Provided the diffuse radiation field is negligible ahead of the star, the flow near the symmetry axis is independent of the rest of the nebula and can therefore be modeled independently for the purposes of determining the self-consistent accretion rate for a wider range of n and v. The results of such modeling are shown in Figure 5 and are compared to the accretion rate assumed in Papers I and II (eq. [1] with $c_s = 10$ km s^{-1} and $\lambda_a = 1$). Clearly preheating of the flow can dramatically reduce the accretion rate and substantially reduce the number of detectable IONSs in the EUV and X-ray sky surveys. For example, using the same ISM model as in Paper II and assuming no dynamical heating of the neutron star population, we have found that the number of detectable sources in the PSPC survey would be $\sim 700 N_8$ for polar cap accretion (a reduction by ~ 5) and $\sim 0.2 N_8$ for isotropic accretion (a reduction by ~ 3000!). The numbers of detectable sources in the WFC survey would be $\sim 1 N_8$ for polar cap accretion and $\sim 0.1 N_8$ for isotropic accretion. The *EUVE* all-sky survey would not be expected to detect any IONSs.[6] These results are subject to some important caveats:

1. The assumption that $c_s = 10$ km s^{-1} was based on the expected temperature of photoionized nebulae which are cooled by collisionally excited metal lines. These metals are at present entirely neglected in our code. Metal line cooling could reduce the temperature and sound speed at the accretion radius, increasing the overall accretion rate. On the other hand, metals could also increase the temperature even further, as they dominate the photoionization opacity for hard photons. We have run some equilibrium nebular models with the photoionization code CLOUDY (Ferland 1993) for stars with temperature and luminosity similar to those discussed above. We generally found that the temperature at distances of $\sim 10^{13}$ cm from the neutron star differed by at most a factor 2 in both directions between static cases with and without metals. However, it is not clear what will happen with nonequilibrium heating and cooling.

2. As discussed in § 3, our treatment of preheating is only phenomenological, but a full hydrodynamical simulation will be necessary to do any better. We have checked the sensitivity to variations in the sound speed around the accretion radius by running the simulations with $R_{\rm acc}$ defined to be double the value given by equation (4). In the case of isotropic accretion, the accretion rate did not change significantly (less than 1%), implying that our phenomenological prescription is robust. Polar cap accretion is more problematic. In both the $n = 1$ cm^{-3} and $n = 100$ cm^{-3} cases, doubling the accretion radius definition increased the resulting converged accretion rate by factors ~ 2–3 for velocities less than 50 km s^{-1}.

3. We have assumed that the ambient gas is neutral well ahead of the star. It is possible for the medium to be fully ionized to begin with for unrelated reasons, e.g., if the star is moving through the warm ionized component of the ISM. Heating by the neutron star radiation field would be drastically reduced in such a case, but the accretion rate would be

[6] These results required calculation of the maximum accretion rate for preheating of cavity material with baryon density of 0.095 cm^{-3}. We found a maximum accretion rate of $\simeq 10^9$ g s^{-1} for both polar cap and isotropic accretion.

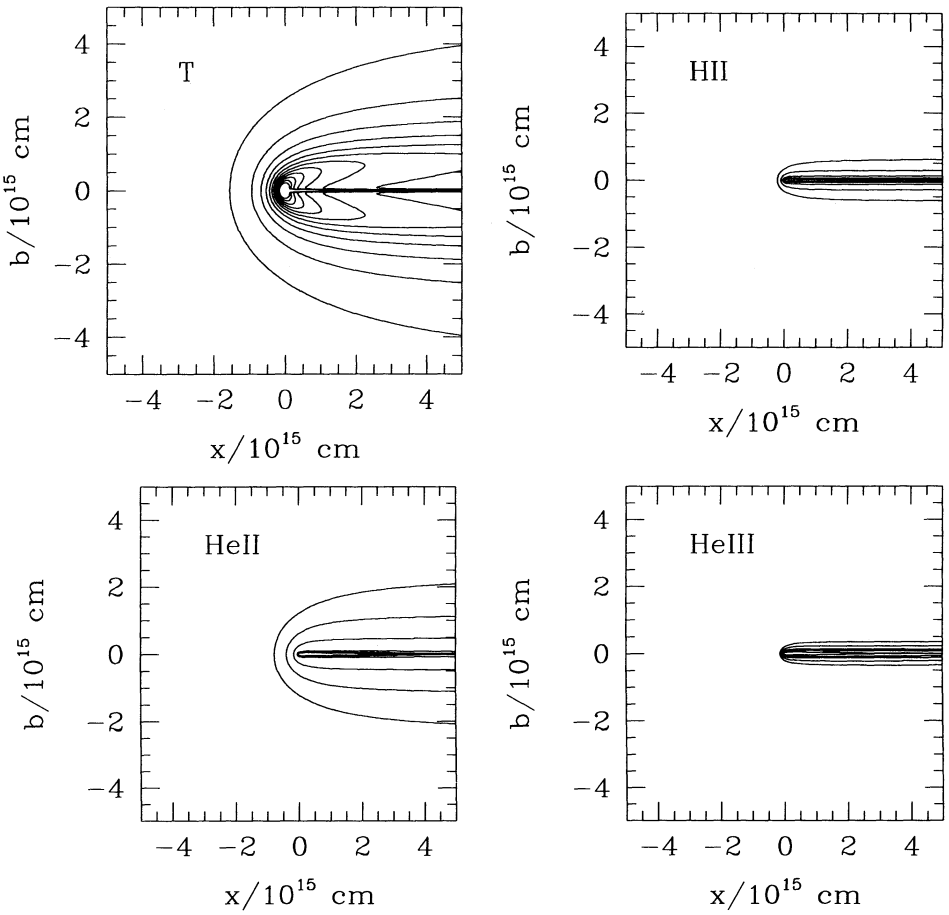

FIG. 4*a*

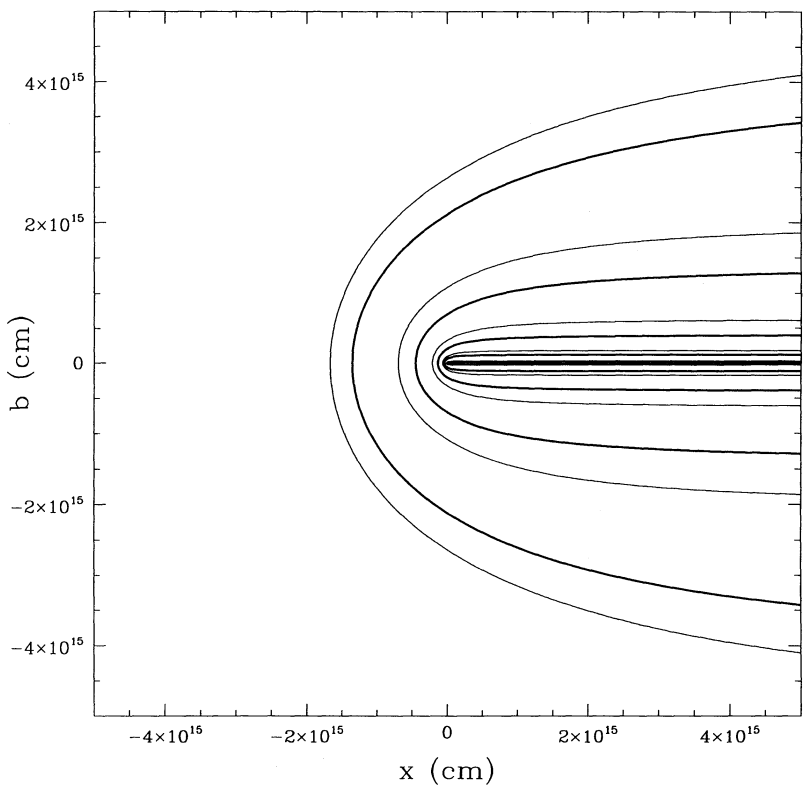

FIG. 4*b*

FIG. 4.—(*a*) Nebular structure for accretion onto a magnetized neutron star with total emitting area 1 km^2, moving at 20 km s^{-1} through a medium $n = 100$ cm^{-3}. Contours are the same as those in Fig. 3*a*. (*b*) Contours of $n_{\rm H\,II}/n_{\rm H}$ at values of 0.01, 0.03, 0.1, 0.3, and 0.9. Light curves are results from the numerical calculations, while heavy curves are the optically thin analytic approximation given by eq. (12).

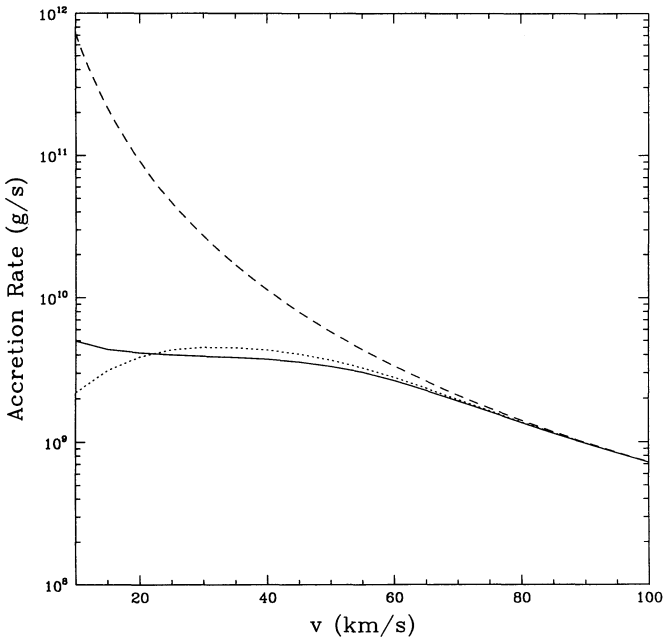

FIG. 5a

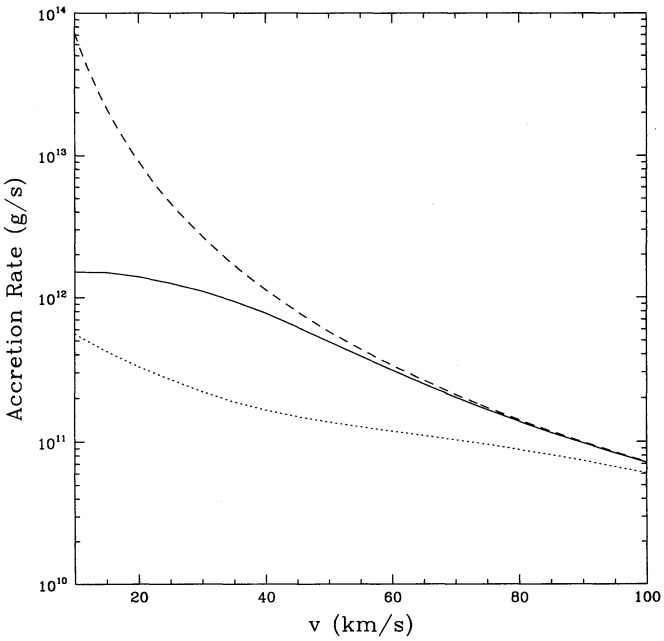

FIG. 5b

FIG. 5.—Self-consistent accretion rate as a function of stellar velocity for (*a*) $n = 1$ cm^{-3} and (*b*) $n = 100$ cm^{-3}. The solid curve is for isotropic accretion ($A = 4\pi R_*^2 = 1.26 \times 10^3$ km^2), the dotted curve is for polar cap accretion ($A = 1$ km^2), and the dashed curve is the accretion rate assumed in Papers I and II.

limited by the relatively low ambient density as compared to that in atomic and molecular clouds.

4. We have assumed throughout this paper that the accretion flow is hydrodynamic, which requires the flow to be ionized at the accretion radius.[7] This is always true for isotropic accretion in the cases we have studied ($n = 1$ and 100 cm^{-3}, $v = 10$–100 km s^{-1}). As illustrated in Figure 6, the flow is only partially ionized at the accretion radius (again defined as $b = R_{acc}$ and $x = 0$) for polar cap accretion. The Bondi-Hoyle accretion rate would then be reduced by a factor comparable to the ionization fraction. This is not significant for $n = 100$ cm^{-3}, and even in the $n = 1$ cm^{-3} case this factor ($\sim \frac{1}{2}$) is comparable to the variation caused by our uncertainty in the accretion radius. The presence of a significant neutral fraction implies that photoionization heating is very important (we find that Compton heating is always small) and can change the temperature of the flow on the scale of the accretion radius. This explains why the accretion rate is sensitive to the choice of accretion radius for polar cap accretion.

5. NEBULAR EMISSION

The reason IONSs are expected to be so faint in the optical is because this band is far into the Rayleigh-Jeans region of their thermal spectra. Reprocessing of the more powerful EUV and soft X-ray radiation could, however, be achieved through the ionization nebula around the IONS itself. This would make these sources much easier to detect and identify.

With this possibility in mind, we have found that, in all our simulations, the cooling is dominated by collisional excitation of hydrogen in the high-temperature region near the neutron star. This suggests that the optical nebular emission will also be concentrated in a compact luminous region around the neutron star, and *not* spread out over the much more extended ionized region. This feature may be crucial for the detectability of IONSs: if the emission were more or less uniform over the entire nebula, the surface brightness would be much lower.

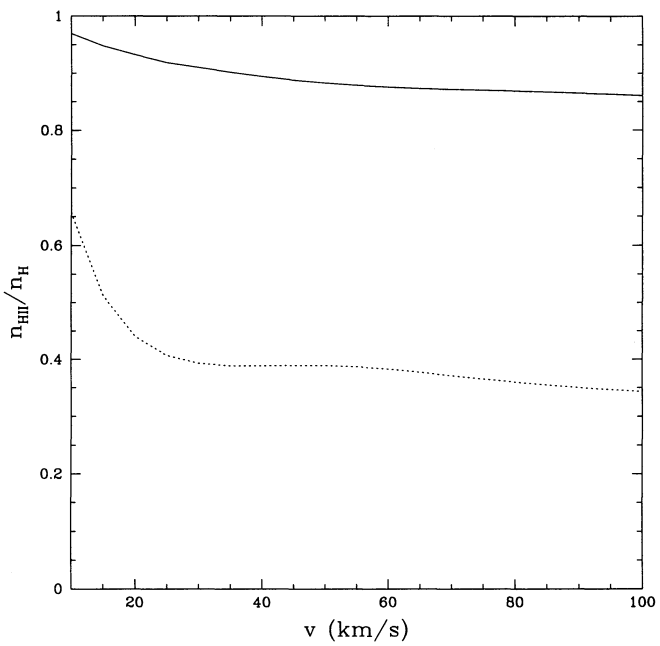

FIG. 6.—Hydrogen ionization fraction at the accretion radius for polar cap accretion ($A = 1$ km^2) and $n = 100$ cm^{-3} (*solid*) and $n = 1$ cm^{-3} (*dotted*). Hydrogen is fully ionized at the accretion radius for the same cases under isotropic accretion.

[7] The collisional mean free path for neutral hydrogen is $\simeq 3 \times 10^{15}$ cm $(n/1$ cm$^{-3})^{-1}(\sigma/3 \times 10^{-16}$ cm$^2)$, where σ is the collision cross section. In all the cases we have calculated, $R_{acc} \sim 10^{13}$ cm for $v = 10$–40 km s^{-1}. Hence, collisions alone might be sufficient to make the flow hydrodynamic for $n \gtrsim 100$ cm^{-3}. However, the flow is always nearly fully ionized at such high densities and low velocities anyway.

Therefore, we have calculated the optical continuum emission for all four cases discussed in § 4 with $v = 20$ km s^{-1}. For the free-free, bound-free, and two-photon H I $2s$–$1s$ processes (the last from recombinations only), we have adopted emission coefficient functions based on interpolating data points found in Osterbrock (1989) and Brown & Mathews (1970). For the two-photon continuum from H I collisional excitation, we have assumed only radiative decay of the $2s$ level and adopted a representative collision strength of $\Omega(1s, 2s) \simeq 0.26$, which is typical at the temperatures where collisional excitation is important (Callaway 1985; Osterbrock 1989). We have neglected H I $2s$–$2p$ collisional transitions, since they are unimportant at these densities, and we have calculated only the emission from the portion of the nebula within the simulation grid. As expected, the two-photon process from collisional excitation of hydrogen completely dominates the optical continuum emission of the nebula.

For the $n = 100$ cm^{-3} cases, the nebular emission in the *UBV* optical bands exceeds that from the neutron star surface itself (by ~ 6 mag in the isotropic case and ~ 3 in the polar cap case). However, for the $n = 1$ cm^{-3} cases, the nebular emission is much fainter than the neutron star itself.

As a concrete example, consider the $v = 20$ km s^{-1}, $n = 100$ cm^{-3} isotropic accretion case. At the distance of the Taurus giant molecular cloud (140 pc), the total continuum flux for this case corresponds to apparent magnitudes of $U = 18.4$, $B = 19.6$, $V = 19.8$, and $R = 19.8$. Most of this radiation arises from collisional excitation cooling in the inner, $T \gtrsim 1.4 \times 10^4$ K region of the nebula. Hence, this radiation will be spread over a region $\sim 2 \times 10^{16}$ cm across (see Fig. 1), corresponding to an angular size of ~ 70 arcsec^2. The surface brightness would be ~ 24 mag arcsec^{-2} in B, while the apparent magnitude of the IONS itself would be $B = 26$ for this case. Diffuse continuum emission should therefore be expected at the sensitivity required to image the IONS itself in the optical.

Emission lines may offer a better prospect for detection, and we have calculated the energy output in the strongest optical recombination lines: The Hα and β lines and the He II λ4686 Fowler line. We assumed a nebula optically thick to low-order Lyman-line photons and neglected collisional transitions, apart from collisional excitation of the $n = 3$ level of hydrogen. The adopted emission coefficients are based on interpolation between the tabulated values listed in Osterbrock (1989). Our results are shown in Table 1. Note that only Hα includes a contribution from collisional excitation; the other emission lines therefore represent lower limits. Production of Hα photons by collisional excitation turns out to be comparable to, and often dominates, the production resulting from recombinations. Hence, emission in this line at least will also be concentrated near the neutron star. This is illustrated in Figure 7, which shows the surface brightness in the Hα line for the $v = 20$ km s^{-1}, $n = 100$ cm^{-3} isotropic accretion case.

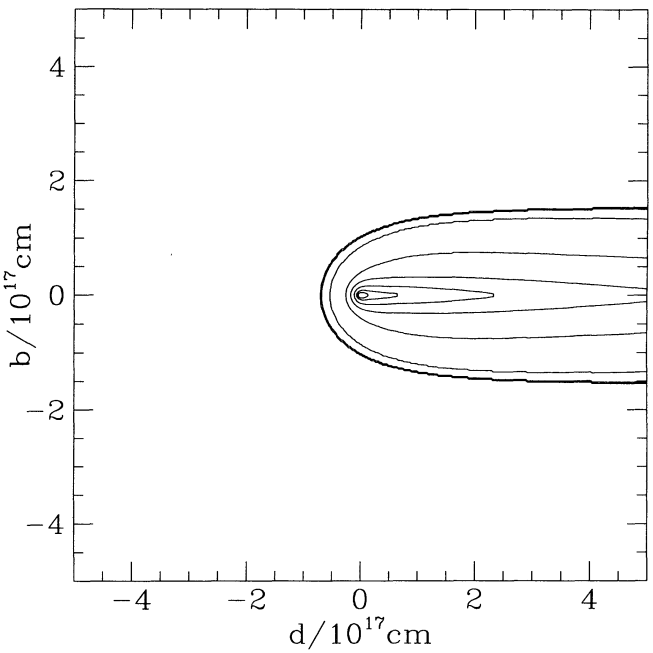

FIG. 7.—Hα surface brightness for isotropic accretion onto a neutron star moving at $v = 20$ km s^{-1} through a medium with $n = 100$ cm^{-3}. Moving out from the neutron star, the contours are 3×10^{-6}, 10^{-6}, 3×10^{-7}, 10^{-7}, 3×10^{-8}, 10^{-8}, 3×10^{-9}, and 10^{-9} ergs cm^{-2} s^{-1} sr^{-1}.

Finally, it is fair to mention that dust and molecules (neglected in our modeling) could produce substantial infrared emission for IONSs accreting in molecular clouds (see Lepp & McCray 1983; Böhringer, Morfill, & Zimmermann 1987).

6. CONCLUSIONS

We have analyzed in considerable detail the structure and properties of cometary H II regions around isolated neutron stars accreting from a pure hydrogen/helium gas. We believe that this is the first time self-consistent, fully nonequilibrium nebulae have been calculated around a moving star. Our results indicate that preheating of the accretion flow may substantially reduce the estimated numbers of detectable IONSs calculated in Papers I and II and in Treves & Colpi (1991). Unfortunately, a large amount of theoretical effort would be necessary to settle this matter definitively, since the problem would involve full hydrodynamical simulations including all the important nonequilibrium atomic processes. We have also found that the reprocessed radiation from cometary H II

TABLE 1

EMISSION FROM SIMULATED PORTION OF NEBULAE[a]

Accretion Mode	n (cm^{-3})	Luminosity from Accretion (ergs s^{-1})	Hα Luminosity (ergs s^{-1})	Hβ Luminosity (ergs s^{-1})	He II λ4686 Luminosity (ergs s^{-1})
Isotropic	1	8×10^{29}	2×10^{24}	5×10^{22}	5×10^{21}
	100	3×10^{32}	2×10^{29}	4×10^{28}	2×10^{28}
Polar Cap ($A = 1$ km^2)	1	7×10^{29}	2×10^{22}	2×10^{19}	6×10^{19}
	100	6×10^{31}	1×10^{25}	3×10^{23}	2×10^{23}

[a] $v = 20$ km s^{-1} in all cases.

regions can enhance the detectability of IONSs at long wavelengths and may provide a method of optically distinguishing them from other types of EUV/X-ray sources.

In addition to the neglect of preheating, the results of Papers I and II relied on the pulsar birth velocity distribution of Narayan & Ostriker (1990). A recent crude analysis by Lyne & Lorimer (1994) has dramatically increased the mean birth velocity of pulsars. A more complete analysis is needed, but taken at face value the larger birth velocites would also substantially reduce the numbers of detectable IONSs.

At the present time, nearby IONSs are being actively searched for. The unidentified *Einstein* source MS 0317.7−6647 has all the characteristics of and has been tentatively identified with an accreting IONS in a cirrus cloud at ~100 pc (Stocke et al. 1995). Walter & Wolk (1994) have argued that an unidentified *ROSAT* soft X-ray source toward the RCrA molecular cloud could plausibly be an example of an accreting IONS. A systematic search of IONSs using *ROSAT* PSPC and *EUVE* observations is also currently underway (Danner & Kulkarni 1994; Shemi 1994). Should new observations strengthen the case for the known IONS candidates, then further theoretical work would become worthwhile and necessary.

We thank N. Panagia for helpful conversations. P. M. was supported in part by NASA grant NAG5-2913. During the course of this work, we learned that similar research is being conducted independently by J. Wang and R. Sutherland.

REFERENCES

Alcock, C., & Illarionov, A. 1980, ApJ, 235, 541
Blaes, O., & Madau, P. 1993, ApJ, 403, 690 (Paper I)
Böhringer, H., Morfill, G. E., & Zimmermann, H. U. 1987, ApJ, 313, 218
Bondi, H. 1952, MNRAS, 112, 195
Brown, R. L., & Mathews, W. G. 1970, ApJ, 160, 939
Callaway, J. 1985, Phys. Rev. A, 32, 775
Cen, R. 1992, ApJS, 78, 341
Colpi, M., Campana, S., & Treves, A. 1993, A&A, 278, 161
Cowie, L. L., Ostriker, J. P., & Stark, A. A. 1978, ApJ, 226, 1041
Danner, R., & Kulkarni, S. 1994, private communication
Ferland, G. J. 1993, CLOUDY 84, Univ. Kentucky Department of Physics and Astronomy Internal Report
Fryxell, B. A., Taam, R. E., & McMillan, S. L. W. 1987, ApJ, 315, 536
Grevesse, N., & Anders, E. 1989, in AIP Conf. Proc. 183, Cosmic Abundances of Matter, ed. C. J. Waddington (New York: AIP), 1
Haardt, F., & Madau, P. 1995, ApJ, submitted
Hunt, R. 1971, MNRAS, 154, 141
———. 1979, MNRAS, 188, 83
Krolik, J. H., & London, R. A. 1983, ApJ, 267, 18
Lepp, S., & McCray, R. 1983, ApJ, 269, 560
Lyne, A. G., & Lorimer, D. R. 1994, Nature, 369, 127
Madau, P., & Blaes, O. 1994, ApJ, 423, 748 (Paper II)
Narayan, R., & Ostriker, J. P. 1990, ApJ, 352, 222
Nobili, L., Turolla, R., & Zampieri, L. 1991, ApJ, 383, 250
Osterbrock, D. E. 1989, Astrophysics of Gaseous Nebulae and Active Galactic Nuclei (Mill Valley: University Science Books)
Ostriker, J. P., McCray, R., Weaver, R., & Yahil, A. 1976, ApJ, 208, L61
Ostriker, J. P., Rees, M. J., & Silk, J. 1970, Astrophys. Lett., 6, 179
Paczyński, B. 1990, ApJ, 348, 485
Raga, A. C. 1986, ApJ, 300, 745
Rappaport, S., Chiang, E., Kallman, T., & Malina, R. 1994, ApJ, 431, 237
Rasiwala, M. 1969, A&A, 1, 431
Reilman, R. F., & Manson, S. T. 1979, ApJS, 40, 815
Ruffert, M. 1994, ApJ, 427, 342
Ruffert, M., & Arnett, D. 1994, ApJ, 427, 351
Shemi, A. 1994, private communication
Shima, E., Matsuda, T., Takeda, H., & Sawada, K. 1985, MNRAS, 217, 367
Shull, J. M., & Van Steenberg, M. E. 1985, ApJ, 298, 268
Shvartsman, V. F. 1971, Soviet Astron., 14, 662
Stocke, J. T., Wang, Q. D., Perlman, E. S., & Donahue, M. E. 1995, AJ, 109, 1199
Taam, R. E., Fu, A., & Fryxell, B. A. 1991, ApJ, 371, 696
Taylor, J. H., Manchester, R. N., & Lyne, A. G. 1993, ApJS, 88, 529
Treves, A., & Colpi, M. 1991, A&A, 241, 107
Verdon, C. P., McCrory, R. L., Epstein, R., Van Horn, H. M., & Savedoff, M. P. 1991, in White Dwarfs, ed. G. Vauclair, & E. Sion (Dordrecht: Kluwer), 295
Walter, F. M., & Wolk, S. J. 1994, BAAS, 26, 1443
Wielen, R. 1977, A&A, 60, 263